Available online at www.sciencedirect.com
ScienceDirect
Journal of Solid State Chemistry 180 (2007) 3082–3092
JOURNAL OF SOLID STATE CHEMISTRY
www.elsevier.com/locate/jssc

Composition- and temperature-dependent phase transitions in 1:3 ordered perovskites $Ba_{4-x}Sr_xNaSb_3O_{12}$

Qingdi Zhou[a], Brendan J. Kennedy[a,*], Margaret M. Elcombe[b], Ray L. Withers[c]

[a]*School of Chemistry, The University of Sydney, Sydney, NSW 2006, Australia*
[b]*Bragg Institute, ANSTO, Menai, NSW 2234, Australia*
[c]*Research School of Chemistry, Australian National University, Canberra, ACT 0200 Australia*

Received 29 May 2007; received in revised form 31 August 2007; accepted 3 September 2007
Available online 11 September 2007

Abstract

A series of 25 members of the 1:3 ordered perovskite family of the type $Ba_{4-x}Sr_xNaSb_3O_{12}$ has been synthesized and their structures determined using synchrotron X-ray and neutron powder diffraction techniques. At room temperature the sample $Ba_4NaSb_3O_{12}$ has a cubic structure in space group $Im\bar{3}m$ with $a = 8.2821(1)$ Å, where the Na and Sb cations are ordered in the octahedral sites but there is no tilting of the $(Na/Sb)O_6$ octahedra. As the average size of the *A*-site cation decreases, through the progressive replacement of Ba by Sr, tilting of the octahedra is introduced firstly lowering the symmetry to tetragonal in $P4/mnc$ then to orthorhombic in *Cmca* and ultimately a monoclinic structure in $P2_1/n$ as seen for $Sr_4NaSb_3O_{12}$ with $a = 8.0960(2)$ Å, $b = 8.0926(2)$ Å, $c = 8.1003(1)$ Å and $\beta = 90.016(2)^\circ$. The powder neutron diffraction studies show that the orthorhombic and tetragonal phases in *Cmca* and $P4/mnc$ co-exist at room temperature for samples with x between 1.5 and 2.

Keywords: 1:3 ordered perovskites; Synchrotron and neutron diffraction

1. Introduction

The archetypal ABO_3 perovskite structure type has a cubic structure in which the *A* cation, located at the centre of the cubic unit cell of length a_p, is coordinated to 12 oxygen anions to form an AO_{12} polyhedron. The *B*-cation is located at each corner of the unit cell and is coordinated with 6 oxygen anions, in a corner-linked BO_6 octahedral framework. The oxygen anions are located at the centre of each face. Remarkably few ABO_3 oxides adopt this simple cubic structure at room temperature, more typically the structure is modified by cooperative tilting of the octahedra, by displacement of the cations from the centre of the octahedra or a combination of the two [1]. These distortions allow combinations of metals to adopt the perovskite structure that otherwise would not be possible. The tendency for any given combination of cations to adopt a distorted variant of the perovskite structure (as opposed to the parent cubic structure) can be quantified by the tolerance factor, t, defined as $t = (r_A + r_O)/[\sqrt{2}(r_B + r_O)]$. In general as t is reduced below unity cooperative tilting of the BO_6 octahedra occurs. The perovskite family is further extended by substitutions, particularly of the *A*- and *B*-site cations. These substitutions can result in significant structural distortions that are not only interesting crystallographically, but are also important since the distortions can have a critical influence on the electronic and magnetic properties of the perovskite materials [1].

When the substitution is on the *B*-site, at certain ratios the two *B*-type cations can preferentially occupy crystallographically distinct sites forming so-called ordered perovskites. Three types of ordered perovskites are known where the ratios of the two *B*-type cations are, 1:1, 1:2 and 1:3. These have the general formulae $A_2B'B''O_6$, $A_3B'B_2''O_9$ and $A_4B'B''_3O_{12}$, respectively. A large number of examples with 1:1 and 1:2 *B*-cation ordering are known, but by

*Corresponding author. Fax: +61 2 9351 3329.
E-mail address: kennedyb@chem.usyd.edu.au (B.J. Kennedy).

0022-4596/$ - see front matter © 2007 Elsevier Inc. All rights reserved.
doi:10.1016/j.jssc.2007.09.004

comparison very few examples with 1:3 ordering have been described, and invariably these contain Sb^V [1]. Recently the antimony containing perovskites $(Na_{0.5}K_{0.5})_{1-x}(LiSb)_xNb_{1-x}O_3$, have attracted attention as promising dielectric materials [2]. The ordered antimony perovskites Ca_2CrSbO_6 and Ba_2LnSbO_6 ($Ln = Y$, Ho) have also attracted interest as a consequence of their magnetic properties and the observation that they can be used as substrates for superconducting thin films [3,4].

The observation that a feature of many so-called smart materials is that they are poised near an instability together with the pervasiveness of perovskites in the solid state has prompted numerous studies of phase transitions in perovskites. These studies generally involve systematic changes in composition, temperature or pressure. For example, in the series of 1:1 ordered perovskites $A_{2-x}Sr_xMWO_6$ (A = Ca, Ba; M = Ni, Co) increasing the effective size of the cation occupying the A-type site by varying the relative amount of alkaline-earth cation present results in a sequence of structures with differing BO_6 octahedral tilting, the cells ranging from monoclinic in $P2_1/n$ with the Glazer [5] tilt system $a^-a^-c^+$ to tetragonal $I4/m$ ($a^0a^0c^-$) and then to cubic $Fm\bar{3}m$ ($a^0a^0a^0$) [6,7]. Here and elsewhere the superscript "−" refers to out-of-phase tilts about the stated axis, "+" to in-phase tilts" and "0" to the absence of tilts. As a second example in both $SrZrO_3$ and $Ba_2Bi_2O_6$ increasing the temperature sequentially removes the tilts. The structure of $SrZrO_3$ evolves from orthorhombic $Pnma$ ($a^+b^-b^-$) to orthorhombic $Imma$ ($a^0b^-b^-$) at 970 K to tetragonal $I4/mcm$ ($a^0a^0c^-$) at 1100 K and finally to cubic $Pm\bar{3}m$ ($a^0a^0a^0$) at 1440 K [8,9]. The transitions in $Ba_2Bi_2O_6$, are from monoclinic $P2_1/n$ ($a^-a^-c^+$) to monoclinic $I2/m$ ($a^0b^-b^-$) at 200 K, rhombohedral $R\bar{3}$ ($a^-a^-a^-$) at 498 K then finally to cubic $Fm\bar{3}m$ ($a^0a^0a^0$) at 893 K [10]. In all these cases the first tilt introduced from the $a^0a^0a^0$ structure involves out-of-phase rotations of the octahedra. Indeed there are very few examples where in-phase tilts occur in the absence of out-of-phase tilts, a well-studied exception being $NaTaO_3$ [11,12].

The preparation and structural properties of the two perovskites $Ba_4NaSb_3O_{12}$ and $Sr_4NaSb_3O_{12}$ have been reported previously with the Ba compound having a ($a^0a^0a^0$) cubic structure [13] whereas the Sr compound is monoclinic with both in-phase and out-of-phase tilts, $a^-b^+c^-$ [14]. The possibility that intermediate tilt systems exist in these types of oxides has not been explored. As part of our ongoing studies of the structures and phase transitions in perovskite oxides, an extensive series of 1:3 ordered perovskite oxides of the type $Ba_{4-x}Sr_x$ $NaSb_3O_{12}$ has been synthesized and the structure of the members determined using synchrotron X-ray and, in selected cases, neutron diffraction. Electron diffraction (ED) has also been employed, where necessary, to confirm unit cell and space group assignments. We show that by varying the effective size of the A-type cation it is possible to stabilize two intermediate phases with differing tilt patterns.

2. Experimental

2.1. Sample preparation

All chemicals were obtained from Sigma-Aldrich and were dried prior to use. A series of 25 oxides of composition $Ba_{4-x}Sr_xNaSb_3O_{12}$ ($0 \leqslant x \leqslant 4$) was prepared by conventional solid-state reaction from stoichiometric amounts of Sb_2O_3 (99.9 + %) with the appropriate metal carbonate ($BaCO_3$ 99.98%, $SrCO_3$ 99.9 + %, Na_2CO_3 99.9%). The samples were heated in air at progressively higher temperatures (780 °C/20 h, 900 °C/60 h, and 1000 °C/60 h) with periodic intermediate regrinding. The samples were contained in covered alumina crucibles to reduce the possibility of sodium loss. The samples were characterized by powder X-ray diffraction using a Shimdazu D6000 diffractometer with scan rates of 1° per minute over the 2θ range 10–100 ° using Cu$K\alpha$ radiation.

2.2. Electron microscopy

Selected samples suitable for examination in the scanning electron microscope (SEM) were examined either as powders or as sintered pellets produced by applying 9–10 tonnes of pressure onto a 10 mm disc. The samples were mounted on standard sample holders and then carbon coated to prevent charging effects. The SEM, and accompanying energy-dispersive X-ray (EDX), analysis was carried out using a Philips XL 30 scanning electron microscope, with a tungsten filament operating at 25 kV, and a working distance of 11 mm. The EDX analysis of elemental composition was performed in conjunction with the imaging process using an EDAX model XL-30 and DX-4eDX ZAF operating system (Version 3.3). Analysis was performed with scan times averaging 90 s.

ED was carried out using a Philips EM 430 transmission electron microscope operating at 300 kV. Samples suitable for TEM work were prepared by the dispersion of finely ground material onto a holey carbon film.

2.3. Synchrotron X-ray diffraction

X-ray diffraction data were collected on the high-resolution Debye Scherrer diffractometer at the Australian National Beamline Facility, Beamline-20B at the Photon Factory, Tsukuba, Japan [15]. The samples were housed in 0.3 mm diameter glass, or for the high temperature measurements quartz, capillaries that were rotated during the measurements. The room temperature data were recorded in the angular range $5 < 2\theta < 85°$, step size 0.01° using X-rays of wavelength 0.82606 Å with two Fuji Image plates being used as detector. Each image plate is 20×40 cm and covers 40° in 2θ. The wavelength was calibrated using Si 640c as a standard. Variable temperature data were collected at a wavelength 0.80123 and 0.99990 Å for $Ba_{1.5}Sr_{2.5}NaSb_3O_{12}$ and $BaSr_3NaSb_3O_{12}$, respectively, using a custom built furnace, at temperatures of up to 800 °C. All measurements were performed under vacuum to minimize air scatter.

2.4. Neutron diffraction

Room temperature powder neutron diffraction data of samples with $x = 0$, 1, 2, 2.5, 3, 4 were recorded in 0.05° steps in the range $10 < 2\theta < 150°$ using neutrons of wavelength 1.4925(2)Å obtained with a Ge monochromators on the high-resolution powder diffractometer (HRPD) at the HIFAR facility, ANSTO [16]. The samples were housed in vanadium containers throughout the measurements.

2.5. Rietveld refinement

Structural parameters were refined by the Rietveld method using the programme RIETICA [17]. A pseudo-Voigt function was used to model the diffraction peaks. The background in the synchrotron diffraction patterns was estimated by linear interpolation between regions where there were no Bragg peaks, whereas a polynomial was used to fit the background in the neutron diffraction data.

3. Results and discussion

3.1. Synthesis and appearance of samples

The preparation of the samples proved relatively straightforward, with traditional ceramic methods yielding polycrystalline samples of the 25 oxides of the type $Ba_{4-x}Sr_xNaSb_3O_{12}$. The colour progressively evolved across the series from a very pale brown in $Ba_4NaSb_3O_{12}$ through cream to white in $Sr_4NaSb_3O_{12}$.

3.2. Room temperature structures

The cell parameters obtained from the structural refinements using synchrotron data are listed in Table 1 and the diffraction patterns for three representative oxides, $Ba_4NaSb_3O_{12}$, $Ba_2Sr_2NaSb_3O_{12}$ and $Sr_4NaSb_3O_{12}$, are presented in Fig. 1. There are large differences between the two different *B*-site cations in terms of formal charge, atomic number (Na = 11, Sb = 51) and ionic radii ($Na^+ = 1.02$ Å, $Sb^{5+} = 0.60$ Å). A series of relatively strong superstructure reflections with the condition $h+k+l = 2n$ was observed in all the oxides, as is illustrated for the selected examples in Fig. 1. These reflections are due to a 1:3 ordering of the Na and Sb cations. The one-dimensional irreducible representation of the parent $Pm\bar{3}m$ space group that is associated with this ordering is $M_1^+(\mathbf{k} = \frac{1}{2}\frac{1}{2}0)$ and this irreducible representation (irrep) results in a doubling of the unit cell size relative to that of the parent perovskite, $a = 2a_p$ [18]. The reflections additional to those of the parent $Pm3m$ structure, observed in the diffraction pattern are referred to as M-point reflections. No evidence was found during the structural

Table 1
Refined cell parameters, equivalent unit cell volume, and space group for the series $Ba_{4-x}Sr_xNaSb_3O_{12}$ at room temperature

Compounds	x	*A*-cation size (Å)	t[a]	a (Å)	b (Å)	c (Å)	β (deg)	Unit Cell volume (Å^3)	Space group
$Sr_4NaSb_3O_{12}$	4	1.44	0.9540	8.0960(2)	8.0926(2)	8.1003(1)	90.016(2)	530.71(2)	$P2_1/n$
$Ba_{0.2}Sr_{3.8}$	3.8	1.4485	0.9569	8.1091(2)	8.1050(2)	8.1152(1)	90.064(1)	533.36(2)	$P2_1/n$
$Ba_{0.4}Sr_{3.6}$	3.6	1.457	0.9597	8.1182(3)	8.1142(2)	8.1281(2)	90.109(1)	535.42(3)	$P2_1/n$
$Ba_{0.5}Sr_{3.5}$	3.5	1.4613	0.9611	8.1236(2)	8.1167(1)	8.1295(2)	90.115(1)	536.03(2)	$P2_1/n$
$Ba_{0.6}Sr_{3.4}$	3.4	1.4655	0.9626	8.1264(3)	8.1210(3)	8.1395(2)	90.166(1)	537.16(3)	$P2_1/n$
$Ba_{0.8}Sr_{3.2}$	3.2	1.474	0.9654	8.1347(3)	8.1273(2)	8.1495(2)	90.197(2)	538.78(3)	$P2_1/n$
$Ba_{1.0}Sr_{3.0}$	3.0	1.4825	0.9683	8.1425(3)	8.1331(2)	8.1632(2)	90.264(2)	540.59(3)	$P2_1/n$
$Ba_{1.2}Sr_{2.8}$	2.8	1.491	0.9711	8.1513(3)	8.1408(2)	8.1738(2)	90.289(2)	542.39(3)	$P2_1/n$
$Ba_{1.4}Sr_{2.6}$	2.6	1.4995	0.9740	11.5702(6)	11.5387(3)	8.1532(3)		1088.49(7)	*Cmca*
$Ba_{1.5}Sr_{2.5}$	2.5	1.5038	0.9754	11.5928(3)	11.5482(3)	8.1597(2)		1092.39(5)	*Cmca*
$Ba_{1.6}Sr_{2.4}$	2.4	1.508	0.9769	11.6001(6)	11.5622(4)	8.1691(3)		1095.65(8)	*Cmca*
$Ba_{1.8}Sr_{2.2}$	2.2	1.5165	0.9797	11.605(1)	11.5826(8)	8.1803(5)		1099.6(2)	*Cmca*
$Ba_{2.0}Sr_{2.0}$[b]	2.0	1.525	0.9826	11.6157(7)	11.5949(5)	8.1879(3)		1102.8(1)	*Cmca*
$Ba_{2.2}Sr_{1.8}$[b]	1.8	1.5335	0.9854	8.2071(4)		8.2178(7)		553.5(1)	*P*4/*mnc*
$Ba_{2.4}Sr_{1.6}$[b]	1.6	1.542	0.9883	8.2169(6)		8.222(1)		555.2(1)	*P*4/*mnc*
$Ba_{2.5}Sr_{1.5}$[b]	1.5	1.5463	0.9897	8.2213(7)		8.223(1)		555.8(1)	*P*4/*mnc*
$Ba_{2.6}Sr_{1.4}$	1.4	1.5505	0.9911	8.2258(4)		8.232(1)		557.0(1)	*P*4/*mnc*
$Ba_{2.8}Sr_{1.2}$	1.2	1.559	0.9940	8.2312(8)		8.239(2)		558.2(1)	*P*4/*mnc*
$Ba_{3.0}Sr_{1.0}$	1.0	1.5675	0.9968	8.2415(3)		8.248(1)		560.2(1)	*P*4/*mnc*
$Ba_{3.2}Sr_{0.8}$	0.8	1.576	0.9997	8.2522(5)		8.255(1)		552.2(1)	*P*4/*mnc*
$Ba_{3.4}Sr_{0.6}$	0.3	1.5845	1.0026	8.2571(1)				562.97(1)	$Im\bar{3}m$
$Ba_{3.5}Sr_{0.5}$	0.5	1.5888	1.0040	8.2629(1)				564.15(1)	$Im\bar{3}m$
$Ba_{3.6}Sr_{0.4}$	0.4	1.593	1.0054	8.2690(1)				565.40(1)	$Im\bar{3}m$
$Ba_{3.8}Sr_{0.2}$	0.2	1.6015	1.0083	8.2766(1)				566.96(1)	$Im\bar{3}m$
$Ba_4NaSb_3O_{12}$	0	1.61	1.0111	8.2821(1)				568.10(1)	$Im\bar{3}m$

The numbers in parentheses are the estimated standard deviations.
[a]Tolerance factor given by $t = (r_A + r_O)/[\sqrt{2}(r_B + r_O)]$.
[b]Two-phase *Cmca* and *P*4/*mnc* observed (see text for discussion).

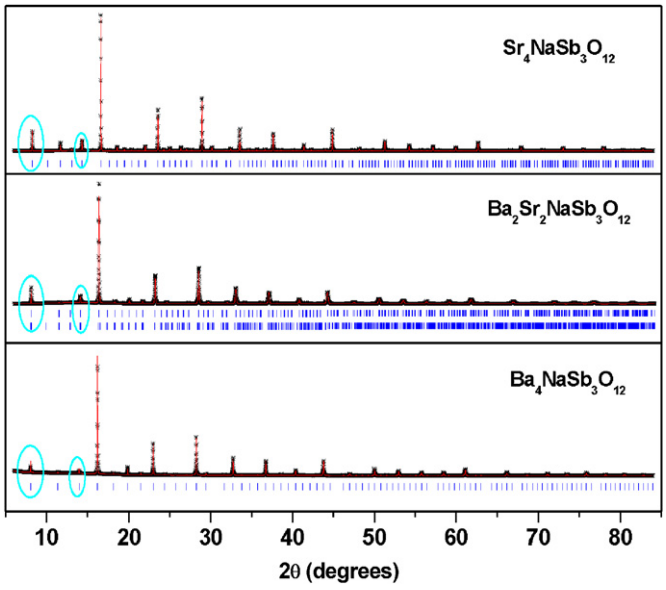

Fig. 1. Observed and calculated synchrotron diffraction patterns for the three oxides $A_4NaSb_3O_{12}$ (A = Ba, Sr) and $Ba_2Sr_2NaSb_3O_{12}$. The markers show the positions of the allowed Bragg reflections. For $Ba_2Sr_2NaSb_3O_{12}$ the upper reflections are from the tetragonal phase and the lower from the orthorhombic phase. The reflections indicated in circles are due to the ordering between the two B-site cations.

refinements for any site mixing and the two different B-site cations appear to be well ordered. The diffraction pattern of $Ba_4NaSb_3O_{12}$ was well fitted to a cubic structure in the space group $Im\bar{3}m$ ($a^0a^0a^0$) with $a = 8.2821(1)$ Å, that is a $2 \times 2 \times 2$ superstructure of the primitive perovskite cell. It is well known that reducing the effective size of the A-type cations can introduce a lowering of symmetry in perovskite oxides. This effect can be quantified by the tolerance factor, $t[t = (r_A + r_O)/[\sqrt{2}(r_B + r_O)]$. No splitting or asymmetry of any the reflections was evident in the diffraction patterns for the five oxides $Ba_{4-x}Sr_xNaSb_3O_{12}$ ($x = 0$, 0.2, 0.4, 0.5 and 0.6) and for these five oxides the structures were refined in space group $Im\bar{3}m$. Across this group the average A-cation radius decreased from 1.610 Å for $x = 0.0$ to 1.585 for $x = 0.6$ with a consequent reduction in the tolerance factor from $t = 1.011$ to 1.000.

At $x = 0.8$, that is for $Ba_{3.2}Sr_{0.8}NaSb_3O_{12}$, slight asymmetry was observed in a number of the high angle reflections in the diffraction pattern, indicating a lowering of symmetry from cubic. Symmetry lowering in perovskites is generally associated with tilting of the octahedra, and for the 1:3 ordered perovskites the appropriate irreps are $M_3^+(\mathbf{k} = \frac{1}{2}\frac{1}{2}0)$ associated with in-phase octahedral tilting and $R_4^+(\mathbf{k} = \frac{1}{2}\frac{1}{2}0)$ associated with out-of-phase tilting [18]. Clearly the subsequent introduction of in-phase tilts to the cubic 1:3 cation ordered structure will not result in any reflections that are diagnostic of in-phase tilting and are distinct from the cation ordering reflections. Conversely the addition of out-of-phase tilts will result in the appearance of additional R-point reflections. This situation is analogous to that seen in the more commonly studied 1:1 ordered double perovskites, where the irreps for cation ordering, $R_1^+(\mathbf{k} = \frac{1}{2}\frac{1}{2}0)$ and for out-of-phase tilting $R_4^+(\mathbf{k} = \frac{1}{2}\frac{1}{2}0)$, allow for the same R-point reflections, meaning these two features are not easily distinguished [19].

In the 1:3 ordered perovskites the intensity of the M-point reflections in the X-ray diffraction patterns will be dominated by the difference in the scattering power of the two cations (Na^+ and Sb^{5+}) with only a very weak contribution from the tilting of the octahedra. R-point reflections from out-of-phase tilting will also be weak in XRD patterns. Close examination of the X-ray diffraction pattern for $Ba_{3.2}Sr_{0.8}NaSb_3O_{12}$ reveals a weak additional reflection near $2\theta = 19.2°$. The intensity of this reflection progressively increased as the Sr content was increased above $x = 0.8$, and this is clearly evident in Fig. 2 for the $x = 1.5$ sample. This peak was indexed as an R-point 1 3 1 reflection demonstrating the presence of out-of-phase tilting of the BO_6 octahedra in addition to the cation ordering. The progressive increase in the intensity of this reflection as the Sr content increases indicates that the magnitude of the associated tilt also increases systematically as the Sr content increases. The increased intensity of the 1 3 1 reflection was accompanied by increased asymmetry, and ultimately resolved splitting, of selected Bragg reflections. This behaviour is indicative of a continuous transformation to a tetragonal structure. Using the group–subgroup relationship for these ordered perovskites established by Howard and Stokes the appropriate space group was identified as $P4/mnc$ ($a^0a^0c^-$) ($2 \times 2 \times 2$) [18]. The patterns of the samples with x between 0.8 and 1.8 (average A-cation radius from 1.576 to 1.534 Å, t = 0.999–0.985) were all fitted using this space group. ED patterns collected for $Ba_3SrNaSb_3O_{12}$ were consistent with this space group assignment. The transition $a^0a^0a^0$–$a^0a^0c^-$ seen here involves the same tilt patterns as is observed in

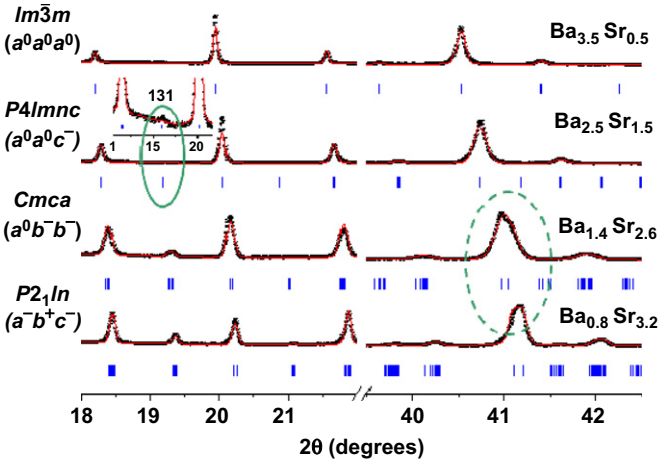

Fig. 2. Potions of the observed and calculated powder X-ray diffraction profiles for $Ba_{4-x}Sr_xNaSb_3O_{12}$ with $x = 0.5$, 1.5, 2.6 and 3.2. The solid circle in the inset for the $x = 1.5$ data highlights the superlattice observed in the tetragonal phase. The dashed circle indicates the reversal in peak intensity at the transition from orthorhombic and monoclinic structure.

the vast majority of both simple ABO_3 and rock-salt ordered 1:1 double perovskites.

As the Sr content was further increased above $x = 1.8$ the shapes of the stronger Bragg reflections become progressively more complex, as is well illustrated by the presence of a doublet of peaks near $2\theta \sim 41^\circ$ in the synchrotron pattern of the $x = 2.6$ sample. This peak was indexed to the 2 4 6 reflection in $Im\bar{3}m$ and must be a singlet in $Im\bar{3}m$ and although it can split in $P4/mnc$ we observe it does not. Clearly a second phase transition has occurred near this composition. Both R- and M-point reflections are clearly evident in the patterns, showing that the out-of-phase tilts are retained and allowing for the possibility of in-phase tilts. Group theory shows there can be a continuous phase transition from $P4/mnc$ $(2 \times 2 \times 2)$ to two lower symmetry options ($P2_1/n$ $[2 \times 2 \times 2]$ and $C2/c$ $[2\sqrt{2} \times 2\sqrt{2} \times 2]$, see Table 2 of [18]). Whilst providing excellent fits to the observed data both models had $\beta \sim 90^\circ$ suggesting the structure may be orthorhombic rather than monoclinic. Whilst somewhat speculative, we note that in a number of ABO_3 perovskites a first order $a^0a^0c^-$–$a^0b^-b^-$ transition is observed. In ABO_3 perovskites this corresponds to $I4/mcm \rightarrow Imma$ [20] transition and in $A_2BB'O_6$ double perovskites this corresponds to the $I4/m \rightarrow I2/m$ transition [19]. It is feasible that the same transition may occur in these ordered perovskites. If this is true, a first order $P4/mnc$ ($a^0a^0c^-$, $2 \times 2 \times 2$) to $Cmca$ ($a^0b^-b^-$, $2\sqrt{2} \times 2\sqrt{2} \times 2$) transition may be expected. This prediction appears to be true, with the fit to the synchrotron X-ray diffraction patterns for $x = 2.0$ being excellent. Subsequently patterns for the samples with $x = 2.6$ and 2.0 (average A-cation radii from 1.499 to 1.525 Å, $t = 0.974$–0.983) were fitted in the orthorhombic space group $Cmca$. The observation of [001] ($= [200]_p$) zone axis EDPs exhibiting the condition $F(hk0) = 0$ unless both h and k are even (see Fig. 3) for the nominally $Cmca$ samples of Table 1 is quite compatible with $Cmca$ but is not compatible with $C2/c$.

In the sample with $x = 2.6$ the reflections near $2\theta \sim 41^\circ$ (indexed as 804 in $Cmca$) is noticeably stronger than the 0 8 4 reflection at the same point. At $x = 2.8$ the relative intensities of these two reflections is reversed, as is apparent in Fig. 2. This behaviour is similar to that seen for first-order phase transitions such as the $I4/mcm$ to $Imma$ transition $SrZrO_3$ [9] and the $R\bar{3}c$ to $Imma$ transition in $PrAlO_3$ [21]. We surmise that a second first-order phase transition has occurred. Again by examination of the

Table 2
EDX chemical compositions versus the theoretical values

Compound	Elemental molar ratio (calc.) Ba:Sr:Na:Sb	Elemental molar ratio (exp.)
$Ba_2Sr_2NaSb_3O_{12}$	2:2:1:3	2.00:2.00:0.58:3.00
$Ba_{2.5}Sr_{1.5}NaSb_3O_{12}$	2.5:1.5:1:3	2.48:1.62:0.77:2.91

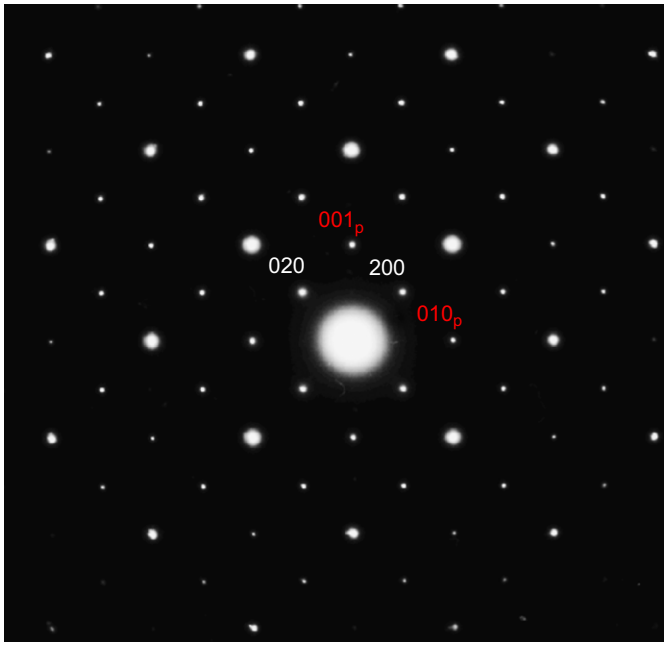

Fig. 3. Electron diffraction pattern of $Ba_2Sr_2NaSb_3O_{12}$. Indexed with respect to a perovskite parent structure (in red) and a $Cmca$, $2\sqrt{2} \times \sqrt{2} \times 2$, supercell (white). The observed pattern with $F(hk0) = 0$ unless h,k *both* even, requires an a glide perpendicular to c. This is compatible with $Cmca$ but not with $C2/c$.

group–subgroup relationships and considering both the metric and presence of superlattice reflections it was concluded that the appropriate space group for the samples with x above 2.8 was monoclinic $P2_1/n$ ($a^-b^+c^-$). For the $x = 2.8$ sample the structure is clearly monoclinic with $\beta = 90.289^\circ$. The diffraction patterns with Sr contents above $x = 2.8$ were all then fitted in this space group.

At this point it should be noted that although the fit to the synchrotron pattern for $Sr_4NaSb_3O_{12}$ in $P2_1/n$ ($a^-b^+c^-$ in a $2 \times 2 \times 2$ superstructure) was excellent the refined values for the cell parameters a, b and c were all approximately equal and the unique monoclinic angle remained very close to 90°. The synchrotron X-ray pattern for this oxide could be equally well fitted in an alternate monoclinic structure in $C2/c$ ($a^-b^-b^-$) or indeed in the same orthorhombic model, $Cmca$, used at lower Sr contents. These models were not satisfactory in the analysis of the $x = 2.8$ sample. Two approaches were taken to confirm that the structure of $Sr_4NaSb_3O_{12}$ was in fact $P2_1/n$ $(2 \times 2 \times 2)$. Firstly an ED study was undertaken. Fig. 4 shows the two typical $\langle 001 \rangle_p$-type zone axis EDPs obtained indexed with respect to a $P2_1/n$ $(2 \times 2 \times 2)$ cell. The observed diffraction data are entirely consistent with $P2_1/n$ space group symmetry and unit cell. Again the presence of the $F(h0l) = 0$ unless $h + l =$ even condition apparent in Fig. 4(b) rules out the possibility of $C2/c$ $(2\sqrt{2} \times 2\sqrt{2} \times 2)$ but not formally $Cmca$ $(2\sqrt{2} \times 2\sqrt{2} \times 2)$. Secondly neutron powder diffraction data were collected in order to provide a more accurate refinement. As stated above, the neutron patterns are expected to be more sensitive to the presence of any in-phase tilts. The results

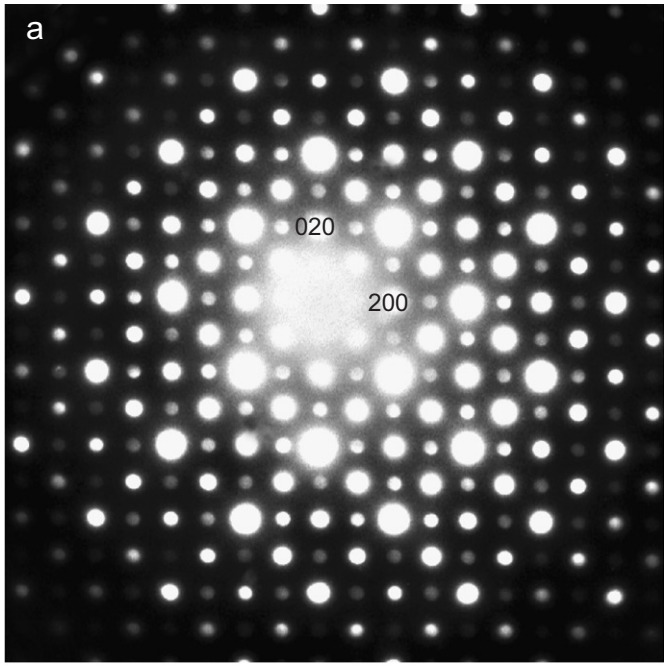

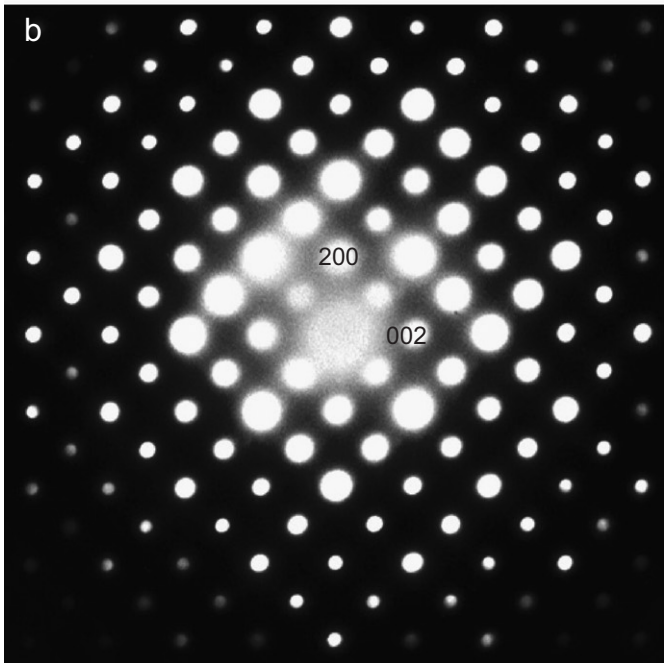

Fig. 4. Electron diffraction patterns of $Sr_4NaSb_3O_{12}$. Consistent with a $P2_1/n$, $a = 2a_p$, $b = 2b_p$, $c = 2c_p$ supercell. No condition is observed for the zero order Laue zone down the [100] or [001] directions and $F(h0l) = 0$ unless $h + l =$ even down [010].

obtained from refinement of neutron data was similar to the refinement for the synchrotron data, and this clearly demonstrates the presence of both in-phase and out-of-phase tilting of the BO_6 octahedra. There is no doubt then that $Sr_4NaSb_3O_{12}$ has space group symmetry $P2_1/n$ and that both in-phase and out-of-phase tilts are present.

The composition dependence of the lattice parameters obtained from the synchrotron diffraction study is shown in Fig. 5. These results can be summarized as the structure

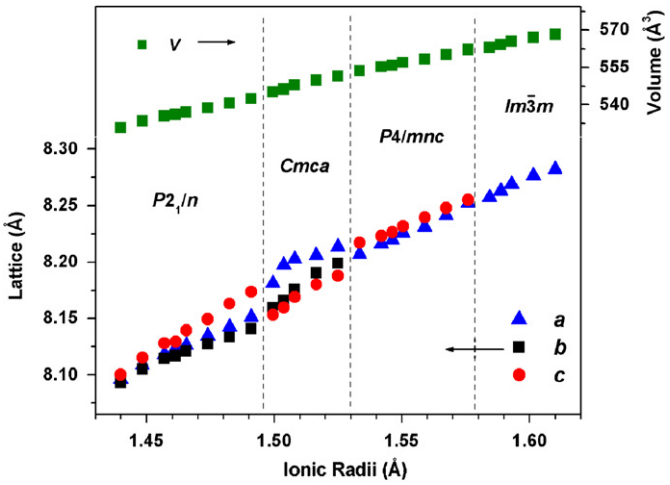

Fig. 5. Variation of lattice parameters and volumes with the average A-cation radius for the series $Ba_{4-x}Sr_xNaSb_3O_{12}$. The reduced lattice parameters for $Cmca$ are $a = a'/\sqrt{2}$, $b = b'/\sqrt{2}$.

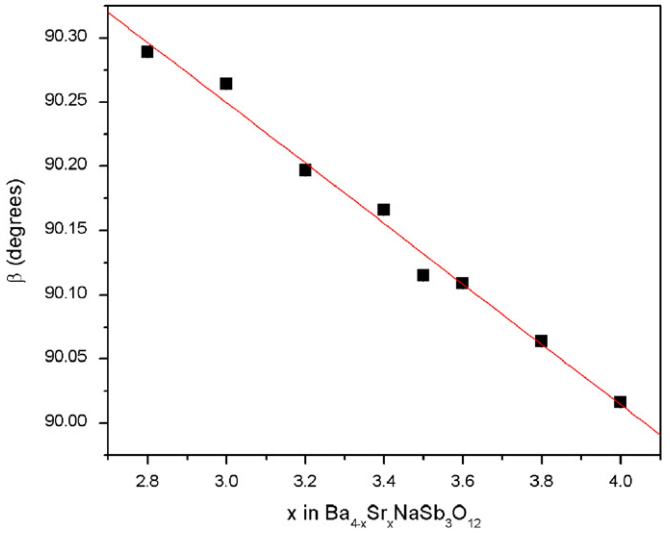

Fig. 6. Composition dependence of the monoclinic angle (β) for the eight members of the series $Ba_{4-x}Sr_xNaSb_3O_{12}$ whose structure is refined in space group $P2_1/n$. Those samples with $x < 2.8$ have $\beta = 0$ indicating the transition must be first order. The solid line is a liner fit to the observed data.

being cubic in $Im\bar{3}m$ for $x \leqslant 0.6$, tetragonal in $P4/mnc$ for $0.8 \leqslant x \leqslant 1.8$, orthorhombic in $Cmca$ for $2.0 \leqslant x \leqslant 2.6$ and monoclinic in $P2_1/n$ for $x > 2.8$. This decrease in symmetry and nature of the tilting pattern is similar to that observed in numerous other perovskite systems. What is unusual is the existence of a first-order $Cmca$–$P2_1/n$ transition near $x = 2.8$. The largest monoclinic distortion, gauged by the monoclinic angle β appears to be at $x = 2.8$ which has $\beta = 90.289(1)^\circ$. Increasing Sr content results in a linear reduction in β to $90.016(2)^\circ$ in $Sr_4NaSb_3O_{12}$ (Fig. 6). Clearly the composition induced $Cmca$–$P2_1/n$ transition near $x = 2.8$ must be first order, despite the fact that it is allowed, under Landau theory, to be continuous. We are, of course, aware that a continuous transition can be first order, however, in all our previous studies of phase

transitions in perovskites, transitions are found to be continuous (or at least very close to this) whenever they are allowed to be.

A second noteworthy feature is the trend for the monoclinic $P2_1/n$ structure to become less distorted, based on lattice parameters, as the Sr content increases. This apparent anomaly is most striking since a stated aim of this work was to examine the use of Sr doping as a means of reducing the tolerance factor, and hence generating more distorted structures. The anomaly is readily explained by noting that the tolerance factor is an indicator of the tendency for a tilting distortion but that this need not be linearly correlated with the lattice parameters. Indeed there are numerous perovskites where the cell metric distortion decreases as the tilt angle increases [22], a striking example being in $Sr_{1-x}Ce_xMnO_3$ [23] (see discussion later in the paper).

A $P4/mnc$ to $Cmca$ transition must be first order and the composition dependence of the lattice parameters are consistent with this. Further there is evidence from the synchrotron diffraction patterns for the co-existence of these two phases over a narrow composition range $1.5 \leqslant x \leqslant 2.0$, such co-existence being a feature of first-order phase transitions. It is, of course, possible that the co-existence of the two phases reflects a miscibility gap in the solid solution. In order to discount this possibility the samples were examined using SEM and associated EDX analyses to ensure they were homogenous. SEM of a number of samples in the two-phase region suggested that all the samples were homogeneous and that there were no apparent regions of Sr or Ba segregation. Furthermore the chemical composition estimated from the EDX analyses on up to nine different areas of a sample invariably yielded Ba:Sr:Sb ratios that were in excellent agreement with the nominal stoichiometry (Table 2). Likewise XRF results showed the Sr:Ba ratios of the bulk samples to be correct. In all cases the Na content estimated from EDX measurements was lower than expected, however we believe this is a consequence of mobility of the Na in the electron beam rather than actual loss of Na from the samples [24,25]. This effect is not apparent in the ED studies where a defocused beam is used. The atomic displacement parameters refined using either the X-ray or neutron diffraction studies are indicative of a fully occupied Na site. In short the samples all appear to be chemically homogenous and the phase segregation observed near $x = 2.0$ is associated with the first-order nature of the transition.

The volume of the cell showed a systematic decrease as the Sr content was increased but there was no indication of any anomalies around any of the critical compositions where the phase transitions occur, showing the transitions to be ferroelastic in nature.

3.3. Neutron diffraction

In order to obtain accurate and precise structures for representative examples of each of the structural variants high-resolution powder neutron patterns were collected for the $x = 0$, 1, 1.5, 2, 3 and 4 samples. The results of these Rietveld analyses are tabulated in Table 3. A feature of the neutron diffraction profiles is the progressive increase in the intensity of the R-point reflections due to out-of-phase tilts, this is illustrated by the 1 3 1 reflection highlighted in Fig. 7. The absence of any such reflections in the neutron diffraction pattern of $Ba_4NaSb_3O_{12}$ is in keeping with the assigned space group ($Im\bar{3}m$, tilt system $a^0a^0a^0$). The cubic structure has a single variable oxygen positional parameter x for O(2) which refines to 0.2710(2). This compares favourable with both the value obtained from the analysis of the synchrotron diffraction pattern, $x = 0.2680(11)$, and that reported previously for this material by Reis and Jacobson [13], $x = 0.2714(1)$. The Na–O distance is 2.244(1) Å and the Sb has a compressed octahedral geometry with four long Sb–O(1) bonds at 2.0700(1) Å and two short 1.8758(14) Å bonds. The corresponding bond valences are 1.82 and 5.09, respectively. A compressed octahedral environment has been observed in a number of other Sb(V) perovskites including Sr_2SbYO_6 [26] although in these other perovskites the difference between the axial and equatorial bond lengths is noticeably smaller than that observed here ($\Delta d = d_{axial} - d_{equatorial} =$ 0.07 Å for Sr_2SbYO_6 cf. 0.192 Å in $Ba_4NaSb_3O_{12}$. This anisotropy in the Sb–O bond distances is thought to be a significant factor in stabilizing the present perovskite oxides. It is somewhat surprising that the NaO_6 octahedra is much more regular, in general it might be expected that the larger Na^+ cation would adopt the more distorted environment.

The magnitude of both the in-phase and out-of-phase tilts in the five oxides $x = 0$, 1, 2, 3, and 4 were calculated from the refined atomic coordinates and these are summarized in Table 4. In the monoclinic $P2_1/n$ structure the tilts for each of the four crystallographically distinct B-type cations are independent of each other, however we find these to be approximately equal, and quote here only the average value. As expected from the observed increase in the intensity of the R-point reflections in the neutron diffraction patterns the magnitude of the in-plane tilts ω increase as the Sr content increases from 1.0° in $Sr_3BaNaSb_3O_{12}$ to 11.0° in $Sr_4NaSb_3O_{12}$. The out-of phase tilts, φ, also increase across the series reaching 6.8° in $Sr_4NaSb_3O_{12}$. These results demonstrate that the distortion of the structure does indeed increase as the Sr content increases, even though the cell metric does not always reflect this.

The bond distances and bond valance sums for the samples studied by neutron diffraction are given in Table 5. As described for $Ba_4NaSb_3O_{12}$ all the samples exhibit a large distortion of the SbO_6 octahedra with Δd being around 0.15 Å. That this distortion persists in the tilted structures demonstrates that it is not a property of the tolerance factor being greater than unity in the cubic structure, as represented by $Ba_4NaSb_3O_{12}$. In all the structures refined using the neutron diffraction data the

Table 3
Structural parameters obtained from the refinements of neutron data for the selected samples $Ba_{4-x}Sr_xNaSb_3O_{12}$ with $x = 0$, 1–4 at room temperature

Compounds		$x = 0$	$x = 1$	$x = 2$		$x = 3$	$x = 4$
				Mixed two phases			
Space group		$Im\bar{3}m$	$P4/mnc$	$P4/mnc$	$Cmca$	$Cmca$	$P2_1/n$
Sr1 (Ba1)	x	0.25	0.2516(5)	0.249(1)	0.25	0.25	0.258(3)
	y	0.25	0.7516(5)	0.749(1)	0.006(2)	−0.001(1)	0.257(5)
	z	0.25	0.25	0.25	0.25	0.25	0.242(2)
	Biso	0.65(2)	0.88(3)	1.28(7)	0.43(8)	1.32(7)	0.95(8)
Sr2 (Ba2)	x				0	0	0.260(3)
	y				0.746(3)	0.743(1)	0.257(3)
	z				0.234(2)	0.239(2)	0.728(2)
	Biso				0.43(8)	1.32(7)	0.95(8)
Na	$x = y = z$	0	0	0	0	0	0
	Biso	1.57(2)	0.9(3)	0.1(4)	0.1(4)	3.4(9)	0.7(6)
Sb1	x	0	0	0	0.5	0.5	0
	y	0.5	0	0	0	0	0
	z	0.5	0.5	0.5	0	0	0.5
	Biso	0.35(2)	0.47(5)	0.6(1)	0.8(1)	0.6(1)	0.6(1)
Sb2	x		0	0	0.25	0.25	0.5
	y		0.5	0.5	0.25	0.25	0
	z		0	0	0	0	0.5
	Biso		0.47(5)	0.6(1)	0.8(1)	0.6(1)	0.6(1)
Sb3	x						0.5
	y						0
	z						0
	Biso						0.6(1)
O1	x	0.25	0	0	0.25	0.25	0.263(5)
	y	0	0.5	0.5	0.271(2)	0.263(1)	−0.031(3)
	z	0.5	0.25	0.25	0.25	0.25	0.019(3)
	Biso	1.05(3)	0.3(3)	0.84(7)	1.66(7)	1.6(2)	1.4(3)
O2	x	0.2710(2)	0	0	0	0	−0.039(3)
	y	0	0	0	−0.026(2)	−0.031(2)	−0.025(3)
	z	0	0.278(2)	0.255(4)	0.258(5)	0.260(3)	0.271(4)
	Biso	0.89(3)	2.6(6)	0.84(7)	1.66(7)	2.8(3)	1.2(5)
O3	x		0.267(1)	0.281(1)	0.131(1)	0.139(1)	0.028(4)
	y		0.0046(8)	−0.001(2)	0.128(2)	0.115(1)	0.263(4)
	z		0	0	0.016(2)	0.020(1)	0.037(4)
	Biso		0.5(2)	0.84(7)	1.66(7)	2.10(2)	1.7(4)
O4	x		0.249(3)	0.247(4)	0.140(1)	0.131(2)	0.531(4)
	y		0.512(1)	0.518(2)	0.113(1)	0.120(2)	0.023(5)
	z		0	0	0.484(1)	0.461(1)	0.267(5)
	Biso		1.8(2)	0.84(7)	1.66(7)	2.0(2)	2.4(5)
O5	x						0.455(3)
	y						0.258(5)
	z						−0.021(3)
	Biso						0.9(3)
O6	x						0.249(3)
	y						0.038(2)
	z						0.469(3)
	Biso						1.(2)
R_w		6.09	5.89	5.18		6.02	4.37
R_{wp}		7.21	7.32	6.23		7.61	5.14
X^2		2.37	2.15	1.58		2.54	1.39

average bond distances and bond valance sums of the Sb cations are unremarkable, except in the orthorhombic structure. It is tempting to use this observation as a suggestion for lower stability of the orthorhombic phase, and this may be related to the persistence of the tetragonal phase at high Sr contents. The BVS for the Na cations are consistently greater than one. It has previously been noted that when very large cations such as alkali or alkaline-earth metals occupy the *B*-site of the perovskite structure unusual BVS can be observed possibly reflecting the polarizability of these large cations [14]. Despite this polarizability, in all cases the NaO_6 geometry is notably more regular than the SbO_6 geometry. Both the BVS for the Na cation and the highly distorted environment of the Sb cation suggest the possibility of some local strains. Such effects can result in local disorder leading to the appearance of diffuse features in the ED patterns. No such features were observed in this work.

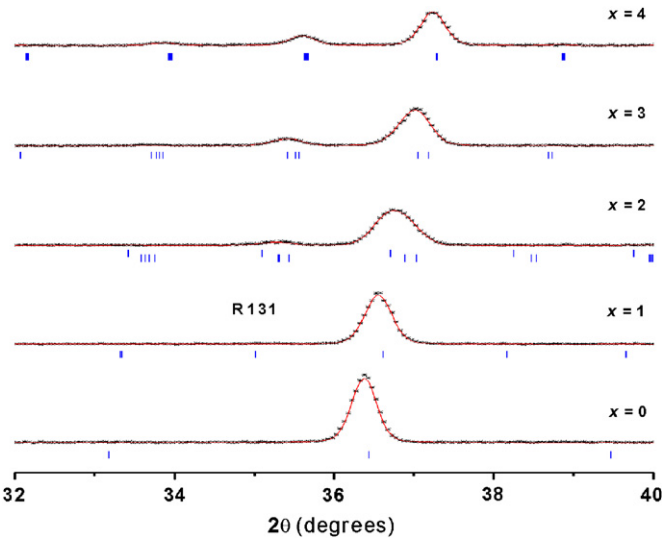

Fig. 7. Potions of the observed and calculated powder neutron diffraction profiles for $Ba_{4-x}Sr_xNaSb_3O_{12}$ with $x = 0$, 1, 2, 3 and 4 showing the evolution in the intensity of the R-point reflections.

Table 4
Average magnitude of the in-phase ω and out-of-phase φ of the tilts (deg) in $Ba_{4-x}Sr_xNaSb_3O_{12}$ estimated from refined atomic coordinates obtained using powder neutron diffraction data

x	ω	φ
0	0	0
1	0	1.0
2	1.0	7.1
3	3.5	7.0
4	6.8	11.0

A second feature obvious in Fig. 7 is the apparent broadness of the majority of the reflections for the two samples with $x = 2$ and 3. This represents two different factors. Firstly the sample with $x = 2$ is two phase, containing both the tetragonal *P*4/*mnc* and orthorhombic *Cmca* phases. Secondly for $x = 3$ the monoclinic distortion is largest, and as noted above this decreases as the Sr content is increases, so that $Sr_4NaSb_3O_{12}$ has pseudo-cubic symmetry. The co-existence of two phases in $Ba_2Sr_2NaSb_3O_{12}$ is demonstrated in Fig. 8. Allowing for these two phase to co-exist in the sample resulted in a significant improvement in the quality of the fit as judged by the various *R*-factors (Table 6). The co-existence of the tetragonal and orthorhombic phases was also observed in the powder neutron diffraction pattern for $Ba_{2.5}Sr_{1.5}NaSb_3O_{12}$.

3.4. Variable temperature structures

Variable temperature synchrotron X-ray diffraction data were collected for the two samples with $x = 2.5$ and 3. At room temperature the sample $Ba_{1.5}Sr_{2.5}NaSb_3O_{12}$ is in space group *Cmca*. Not unexpectedly the symmetry

Table 5
Bond distances and bond valance sum obtained from the refinements of neutron patterns for selected samples

Compound	Space group	*M*–O	Distance (Å) (cal.)[a]	Distance (Å) (exp.)	BVS[b]
$Ba_4NaSb_3O_{12}$	$Im\bar{3}Im$	Ba–O	3.01	2.9301(1)	2.10
		Na–O	2.42	2.244(1)	1.82
		Sb–O	2.00	2.012(1)	5.09
$Ba_2Sr_2NaSb_3O_{12}$ (two-phase co-exist)	*P*4/*mnc*	Ba/Sr–O	2.925[c]	2.93(1)	1.77
		Na–O	2.42	2.24(1)	1.91
		Sb–O	2.00	2.02(1)	5.11
	Cmca	Ba/Sr–O	2.925[c]	2.90(2)	2.02
		Na–O	2.42	2.12(3)	2.50
		Sb–O	2.00	2.04(2)	4.61
$Sr_4NaSb_3O_{12}$	$P2_1/n$	Sr–O	2.84	2.88(3)	1.95
		Na–O	2.42	2.18(3)	2.18
		Sb–O	2.00	2.01(3)	5.09

[a]Calculated using Shannon ionic radii (R.D. Shannon, Acta Crystallogr. A32 (1976) 751–767).
[b]Calculated using equation $s = \exp[(r_0–r)/B]$ (I.D. Brown, D. Altermatt, Acta Crystallogr. B41 (1985) 244–247).
[c]Average bond distance of Ba–O and Sr–O.

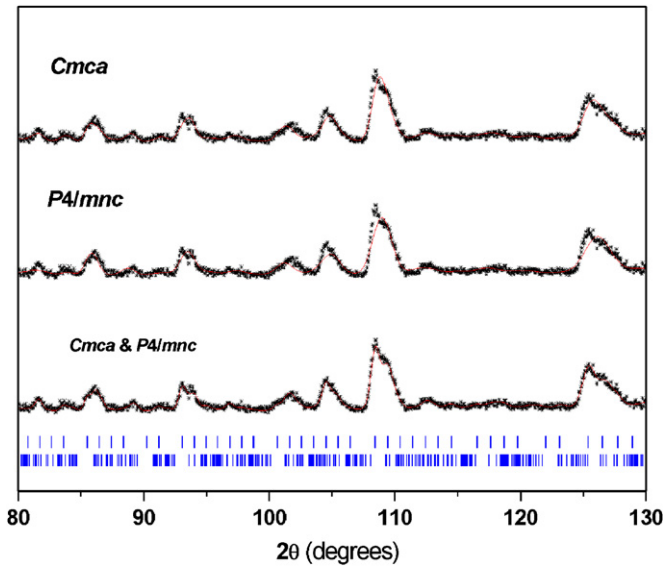

Fig. 8. Potions of the observed and calculated powder neutron diffraction profiles for $Ba_2Sr_2NaSb_3O_{12}$: fitted in single *Cmca* (upper) with $R_p = 6.38$, $R_{wp} = 7.92$, $X^2 = 2.54$; and *P4/mnc* (middle) with $R_p = 7.57$, $R_{wp} = 9.33$, $X^2 = 3.57$. The successful fit using a two-phase *Cmca* and *P4/mnc* model with $R_p = 5.18$, $R_{wp} = 6.23$, $X^2 = 1.58$.

Table 6
Comparison of *R*-factor obtained from the refinements for selected neutron data using single- or two-phase model

Space group	$Ba_2Sr_2NaSb_3O_{12}$			$Ba_{2.5}Sr_{1.5}NaSb_3O_{12}$		
	R_p	R_{wp}	X^2	R_p	R_{wp}	X^2
P4/mnc	7.57	9.33	3.57	6.40	9.03	14.22
Cmca	6.38	7.92	2.54	5.37	7.24	9.18
P4/mnc + Cmca	5.18	6.23	1.58	3.66	4.57	3.67

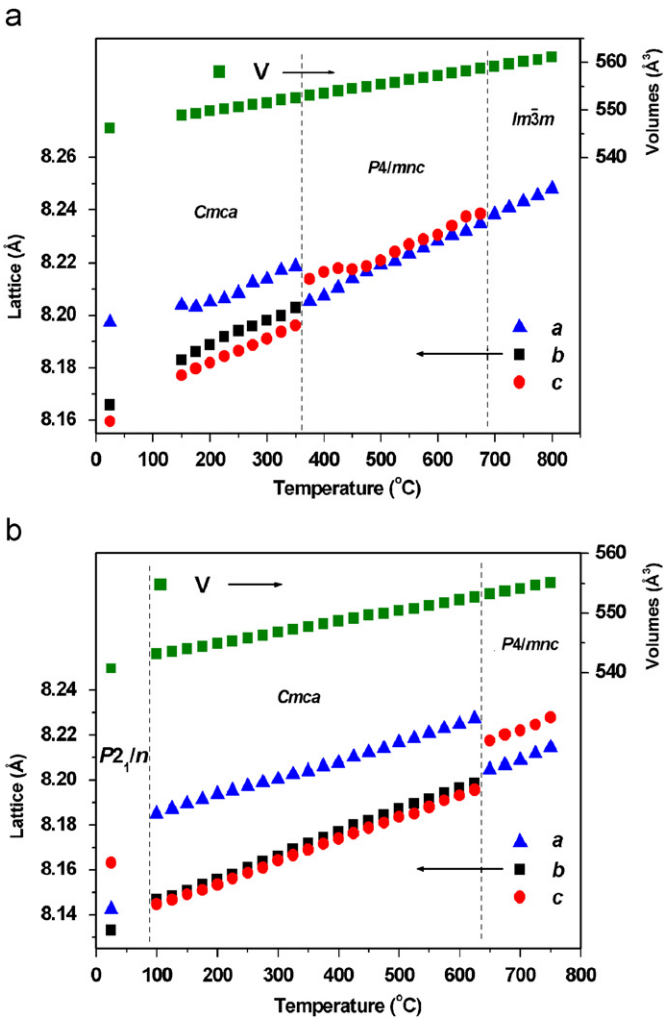

Fig. 9. Variation of lattice parameters and volumes versus temperature obtained from the refinements of synchrotron data for samples (A) $Ba_{1.5}Sr_{2.5}NaSb_3O_{12}$ and (B) $BaSr_3NaSb_3O_{12}$. The reduced lattice parameters for *Cmca* are $a = a'/\sqrt{2}$, $b = b'/\sqrt{2}$.

increased as the temperature increased. Near 350 °C the orthorhombic structure transformed to the tetragonal *P4/mnc* as shown in Fig. 9, although establishing the precise temperature of this was difficult due to the co-existence of the two phases. The refinements suggested there is a significant discontinuity in the lattice parameters associated with this phase transition. Once the tetragonal structure was formed the tetragonal splitting was observed to slowly decrease until there was no apparent splitting or asymmetry in any of the reflections in the diffraction patterns recorded above 675 °C. All such patterns were well fitted using the cubic *Im*$\bar{3}$*m* structure. Although the individual lattice parameters showed a discontinuity at the *Cmca–P4/mnc* transition no such discontinuity was observed in the temperature dependence of the volume. For $BaSr_3NaSb_3O_{12}$ the transition from orthorhombic to tetragonal was found at higher temperatures at ~650 °C and again an apparent discontinuity on the lattice parameters that is indicative of a first-order structure phase transition (Fig. 9). The diffraction data indicates that this remains tetragonal to the highest temperature examined, 750 °C. Once again the temperature dependence of the volume does not show any indication of a discontinuity associated with the phase transition. Whilst limited data was collected it seems reasonable to postulate that the same sequence of phases exist in the variable temperature studies as observed in the composition-dependent studies.

4. Conclusions

The present work appears to be the first comprehensive study of the structures formed in the 1:3 ordered $A_4B'B''_3O_{12}$ perovskites. As observed in numerous other perovskite oxides reducing (the summary below is for increasing cation size the size of the *A*-site cation induces tilting of the BO_6 octahedra. The sequence of structures seen in $Ba_{4-x}Sr_xNaSb_3O_{12}$ can be summarized as

$$P2_1/n \xrightarrow{rA=1.491\ \text{Å}} Cmca \xrightarrow{rA=1.525\ \text{Å}} P4/mnc \xrightarrow{rA=1.576\ \text{Å}} Im\bar{3}m,$$

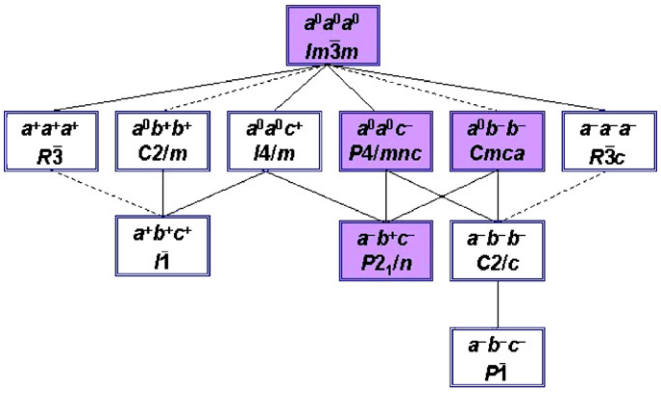

Fig. 10. Group and subgroup relationships, dashed line joining a group to its subgroup indicates that the corresponding phase transition is (required by Landau theory) to be first order and solid line indicates that the corresponding phase transition is to be continuous. Where there is no line joining two sub-groups (e.g. $P4/mnc$ and $Cmca$) the transition must be first order.

where r_A is the effective size of the A while the effective size of the A-type cation. As the cation radius increased by the addition of Ba the tilting of the BO_6 octahedra decreased and ultimately a transition from monoclinic $P2_1/n$ to orthorhombic $Cmca$ was observed. Although such a transition is allowed to be continuous, we find that this is first order. As the A-cation size further increased transitions to the higher symmetry structure, tetragonal $P4/mnc$ and finally cubic $Im\bar{3}m$ were observed. These experimental results are consistent with a group theoretical analysis of phase transitions in 1:3 ordered perovskites as shown in Fig. 10. The distortion of the SbO_6 octahedra in these structures is remarkable, showing a large tetragonal compression. It is possible that, as first postulated by Alonso et al. [14], that this feature contributes to the formation of the 1:3 ordering.

Acknowledgments

The support and encouragement of Dr. Chris Howard in this work is gratefully acknowledged. This work was supported by a grant from the Australia Research Council. Synchrotron diffraction measurements were performed at the Australian National Beamline Facility with support from the Australian Synchrotron Research Programme, which is funded by the Commonwealth of Australia under the Major National Research Facilities Programme. The neutron diffraction measurements were supported by the Australian Institute of Nuclear Science and Engineering. The authors also gratefully acknowledge Dr. James Hester for assistance at the ANBF.

References

[1] R.H. Mitchell, Perovskites: Modern and Ancient, Almaz Press, Ontario, Canada, 2002.
[2] G.Z. Zang, J.F. Wang, H.C. Chen, W.B. Su, C.M. Wang, P. Qi, B.Q. Ming, J. Du, L.M. Zheng, Appl. Phys. Lett. 88 (2006) 212908.
[3] M. Retuerto, J.A. Alonso, M. García-Hernández, M.J. Martínez-Lope, Solid State Commun. 139 (2006) 19.
[4] J.A. Alonso, C. Cascales, P. García, I. Rasines, J. Solid State Chem. 128 (1997) 247.
[5] A.M. Glazer, Acta Crystallogr. B 28 (1972) 3384;
A.M. Glazer, Acta Crystallogr. B 31 (1975) 756.
[6] Q. Zhou, B.J. Kennedy, C.J. Howard, M.M. Elcombe, A.J. Studer, Chem. Mater. 17 (2005) 5357.
[7] Q. Zhou, B.J. Kennedy, M.M. Elcombe, J. Solid State Chem. 180 (2007) 541.
[8] B.J. Kennedy, C.J. Howard, B.C. Chakoumakos, Phys. Rev. B 59 (1999) 4023.
[9] C.J. Howard, K.S. Knight, B.J. Kennedy, E.H. Kisi, J. Phys. C: Condens. Matter 12 (2000) L677.
[10] B.J. Kennedy, C.J. Howard, K.S. Knight, Z. Zhang, Q. Zhou, Acta Crystallogr. B62 (2006) 537.
[11] C.N.W. Darlington, K.S. Knight, Acta Crystallogr. B55 (1999) 24.
[12] B.J. Kennedy, A.K. Prodjosantoso, C.J. Howard, J. Phys. C: Condens. Matter 11 (1999) 6319.
[13] K.P. Reis, A.J. Jacobson, Acta Crystallogr. C49 (1993) 1585.
[14] J.A. Alonso, E. Mzayek, I. Rasines, J. Solid State Chem. 84 (1990) 16.
[15] T.M. Sabine, B.J. Kennedy, R.F. Garrett, G.J. Foran, D.J. Cookson, J. Appl. Crystallogr. 28 (1995) 513.
[16] C.J. Howard, C.J. Ball, R.L. Davis, M.M. Elcombe, Aust. J. Phys. 36 (1983) 507.
[17] C.J. Howard, B.A. Hunter, A Computer Program for Rietveld Analysis of X-ray and Neutron Powder Diffraction Patterns, Lucas Heights Research Laboratories, NSW, Australia, 1998, pp. 1–27.
[18] C.J. Howard, H.T. Stokes, Acta Crystallogr. B60 (2004) 674.
[19] C.J. Howard, B.J. Kennedy, P.M. Woodward, Acta Crystallogr. B59 (2003) 463.
[20] C.J. Howard, H.T. Stokes, Acta Crystallogr. B54 (1998) 782.
[21] M.A. Carpenter, C.J. Howard, B.J. Kennedy, K.S. Knight, Phys. Rev. B 72 (2005) 024118.
[22] C.J. Ball, B.D. Begg, D.J. Cookson, G.J. Thorogood, E.R. Vance, J. Solid State Chem. 139 (1998) 238.
[23] V. Caignaert, F. Millange, M. Hervieu, E. Suard, B. Raveau, Solid State Commun. 99 (1996) 173.
[24] B. Bühn, A.H. Rankin, M. Radtke, M. Haller, A. Knöchel, Am. Mineral. 84 (1999) 1117.
[25] O. Nakamura, Y. Saito, M. Yamada, M. Nakagawa, Solid State Ion. 79 (1995) 111.
[26] W.T. Fu, D.J.W. Ijdo, Solid State Commun. 134 (2005) 177.